

William A. Copen, MD
Lee H. Schwamm, MD
R. Gilberto González, MD,
PhD
Ona Wu, MS
Carla B. Harmath, MD
Pamela W. Schaefer, MD
Walter J. Koroshetz, MD
A. Gregory Sorensen, MD

Index terms:

Aging
Brain, diffusion, 13.12144
Brain, infarction, 13.4352
Brain, MR, 13.121411
Magnetic resonance (MR), diffusion
study, 13.12144

Published online: September 18, 2001
10.1148/radiol.2211001397
Radiology 2001; 221:27–34

Abbreviations:

ADC = apparent diffusion coefficient
rADC = relative ADC
ROI = region of interest

¹ From Harvard Medical School (W.A.C., L.H.S., R.G.G., P.W.S., W.J.K., A.G.S.); Division of Neuroradiology (R.G.G., P.W.S., A.G.S.), NMR Center (W.A.C., R.G.G., O.W., C.B.H., P.W.S., A.G.S.), Department of Neurology (L.H.S., W.J.K.), Massachusetts General Hospital, 13th St, Bldg 149, mail code 2301, Boston, MA 02129. Received Aug 15, 2000; revision requested Sep 26; final revision received Mar 14, 2001; accepted Apr 6. Supported by Public Health Service grant R01NS8477-01 and grant 5P41-RR14075. W.A.C. supported in part by American Heart Association Student Scholarship in Cerebrovascular Disease and educational stipend from Harvard Medical School Office of Enrichment Programs. **Address correspondence to A.G.S.** (e-mail: sorensen@nmr.mgh.harvard.edu).
© RSNA, 2001

Author contributions:

Guarantors of integrity of entire study, W.A.C., A.G.S.; study concepts, W.A.C., L.H.S., R.G.G., O.W., P.W.S., W.J.K., A.G.S.; study design, C.B.H., W.A.C., W.J.K., A.G.S.; literature research, W.A.C., L.H.S., O.W., W.J.K.; clinical studies, W.A.C., L.H.S., O.W., C.B.H., A.G.S.; data acquisition, L.H.S., R.G.G., P.W.S., O.W., W.J.K., A.G.S.; data analysis/interpretation, W.A.C., L.H.S., C.B.H.; statistical analysis, W.A.C., O.W.; manuscript preparation, all authors; manuscript definition of intellectual content, W.A.C., L.H.S., R.G.G., O.W., P.W.S., W.J.K., A.G.S.; manuscript editing, revision/review, and final version approval, all authors.

Ischemic Stroke: Effects of Etiology and Patient Age on the Time Course of the Core Apparent Diffusion Coefficient¹

PURPOSE: To determine whether the evolution of the core apparent diffusion coefficient (ADC) of water in ischemic stroke varies with patient age or infarct etiology.

MATERIALS AND METHODS: One hundred forty-seven patients with stroke underwent 236 diffusion-weighted magnetic resonance imaging examinations. Etiologies of lesions were classified according to predefined criteria; in 224 images, the diagnosis of lacune could be firmly established or excluded. ADC was measured in the center of each lesion and in contralateral normal-appearing brain. A model was used to describe the time course of relative ADC (rADC), which is calculated by dividing the lesion ADC by the contralateral ADC, and to test for age- or etiology-related differences in this time course.

RESULTS: Transition from decreasing to increasing rADC was estimated at 18.5 hours after stroke onset. In subgroup analysis, transition was earlier in nonlacunes than in lacunes ($P = .02$). There was a trend toward earlier transition in patients older than the median age of 66.0 years, compared with younger patients ($P = .06$). Pseudonormalization was estimated at 216 hours. Among nonlacunes, the rate of subsequent rADC increase was more rapid in younger patients than in older patients ($P = .001$). Within the smaller sample of lacunes, however, no significant age-related difference in this rate was found.

CONCLUSION: Differences in ADC depending on the patient's age and infarct etiology suggest differing rates of ADC progression.

The risks and benefits of new therapies for ischemic stroke are likely to depend on the degree of ischemic damage that has already taken place before treatment. Diffusion-weighted magnetic resonance (MR) imaging may provide a more direct way of measuring the extent of tissue injury than can be obtained with clinical history or other common imaging modalities. This is partly because diffusion-weighted MR imaging can be used to measure the apparent diffusion coefficient (ADC) of water within imaged tissue. The ability of diffusion-weighted MR imaging to depict changes in ADC accounts for its superior ability to assist in the detection of hyperacute ischemic stroke (1–3). ADC decreases within the first few minutes of ischemic insult (4–8). Thereafter, ADC remains abnormally decreased for some time before increasing to a normal level. This latter process has been called “pseudonormalization” to reflect the fact that the tissue is damaged and probably nonviable and is typically characterized by a normal ADC but elevated signal intensity at T2-weighted MR imaging. After pseudonormalization, ADC continues to increase and remains permanently elevated.

This sequence of ADC changes in stroke has been well documented (9–16) and is thought to reflect various stages of ischemic injury. The process most often invoked to explain the acute reduction in ADC is cytotoxic edema, that is, a shift of water from the

extracellular space into cells, which occurs as a result of accumulation of intracellular ions (4,17–23). Other proposed mechanisms include a decrease in the diffusivity of intracellular water (24) or in both intracellular and extracellular water (25), increased tortuosity of extracellular diffusion paths as a result of cellular swelling (22), and reduced permeability of cell membranes to water (26). After ADC reaches a minimum, its gradual increase to pseudonormal and then elevated levels is thought to reflect a sequence of histopathologic changes beginning with vasogenic edema and progressing through loss of cell membrane integrity, gliosis, and, ultimately, cyst formation (27–29).

Because the time course of ADC changes may reflect progression of tissue through different stages of ischemic damage (28–32), differences in the rates of evolution of ADC may imply different therapeutic windows for different types of ischemic lesions. We hypothesized that the evolution of ADC may proceed at different rates in patients whose infarcts are of lacunar versus nonlacunar etiology, because these two types of infarcts have different pathophysiologic mechanisms. Most lacunes are thought to result from occlusion of small penetrating arteries by lipohyalinosis, a particular variety of microatheromatous lesion. Nonlacunar infarctions, however, usually result from thromboembolic events that originate in larger vessels or the heart. Lacunar etiology has been associated with more favorable clinical outcome (33,34).

We also hypothesized that a patient's age may influence the time course of ADC, because of previous findings of age-related differences in stroke outcome (35,36).

The purpose of this study was to determine whether the evolution of the core ADC of water in ischemic stroke varies with patient age or infarct etiology.

MATERIALS AND METHODS

Patient Selection

Though patients provided informed consent, when necessary, at the time of imaging, informed consent for retrospective review of their records was not required by our institutional review board for this study.

Radiology reports were retrospectively reviewed in all 3,180 patients who underwent MR imaging examinations including diffusion-weighted MR imaging at our hospital from November 1995 through July

1997. MR images included in this study were selected from the 905 reports (in 673 patients) that mentioned a lesion believed to be of ischemic etiology. Because our goal was to identify lesions with known time of onset, we excluded the 356 examinations accompanied by reports that described lesions that were incidental discoveries or that were likely to be of gradual or uncertain onset (eg, "diffuse periventricular white matter changes"). Medical records from the remaining patients were reviewed to confirm that each patient had received a diagnosis of completed ischemic stroke, with a neurologic deficit that persisted until the time of discharge and that was attributable to the lesion described in the radiology report. Ten examinations were eliminated because patients received thrombolytic (5) or experimental neuroprotective (5) therapy before the examination.

Of the 539 examinations identified with this method, 70 were excluded because of other diagnoses that could have explained the patients' neurologic deficits or that could have unusually influenced the time course of ADC, including intracranial mass lesions ($n = 35$), infectious processes ($n = 11$), metabolic encephalopathy ($n = 9$), vasculitis or other autoimmune disease ($n = 7$), severe hydrocephalus ($n = 1$), air embolism ($n = 2$), fat embolism ($n = 1$), and moyamoya disease ($n = 2$). Of the 70 examinations, two were eliminated because one patient received more than one of these diagnoses; 14 additional examinations were excluded because the patients' strokes were posttraumatic.

For the remaining 455 examinations, we determined from medical records the time when each patient was last seen at baseline status before the stroke occurred and the time when the new neurologic deficit was recognized. For patients without witnessed stroke onset, the time halfway between these two times was taken to be the time of occurrence of the stroke for the purpose of data analysis. Each image was included in the study only if the maximum possible error of the elapsed time between stroke onset and MR imaging was less than 5% of that time. For example, if a patient was last seen without a neurologic deficit at 8 AM and was first noted to have a deficit at 10 AM, then the estimated time of stroke onset would be 9 AM, and the maximum error of that estimate would be 1 hour. An image in this patient would be included only if it was obtained more than 20 hours after 9 AM ($20 \text{ hours} \times 5\% = 1 \text{ hour maximum error}$); 197 images were eliminated be-

TABLE 1
Etologic Classification of 236 Images according to Criteria Used in the Trial of ORG 10172 in Acute Stroke Treatment (TOAST)

Category and Description	No. of Images
1, large artery atherosclerosis	47
2, cardiogenic embolism	30
3, small-vessel occlusion (lacune)	41
4, other known etiology	36
5, unknown etiology	82

cause the time of onset of symptoms could not be estimated with this level of precision.

Of the remaining 258 examinations, four were eliminated because severe artifacts due to patient motion or technical factors made it impossible to measure ADC accurately. Thirteen examinations were eliminated because a lesion could not be definitely identified. Another five examinations were eliminated because the lesions were smaller than the 3×3 -voxel region of interest (ROI) used in this study. This left 236 examinations in 147 patients that were included. Forty-one patients underwent imaging at multiple times, and the number of examinations per patient ranged from one to seven, with a mean of 1.6. Patient age ranged from 20.1 to 91.6 years (mean age, 62.2 years; median age, 66.0 years). For age-related analysis, patients were classified as young (≤ 66.0 years) or old (> 66.0 years); 90 (61%) of 147 patients were male, and 57 (39%) were female. Of the 236 images, 143 (61%) were obtained in male patients, and 93 (39%) were obtained in female patients.

Determination of Stroke Etiology

Each patient's stroke was assigned to one of the five etiologic categories defined for use in the Trial of ORG 10172 in Acute Stroke Treatment, or TOAST (37). The number of images assigned to each category is listed in Table 1. All patients assigned to the lacune (small-vessel occlusion) category had brainstem or subcortical hemispheric lesions with a diameter of less than 15 mm on the first available image; no evidence of a high-risk source of cardiogenic embolism; and no evidence of greater than 50% stenosis of an ipsilateral carotid, vertebral, or basilar artery. Medical records in these patients were reviewed by a neurologist who specializes in stroke (L.H.S.) to confirm that their clinical histories and find-

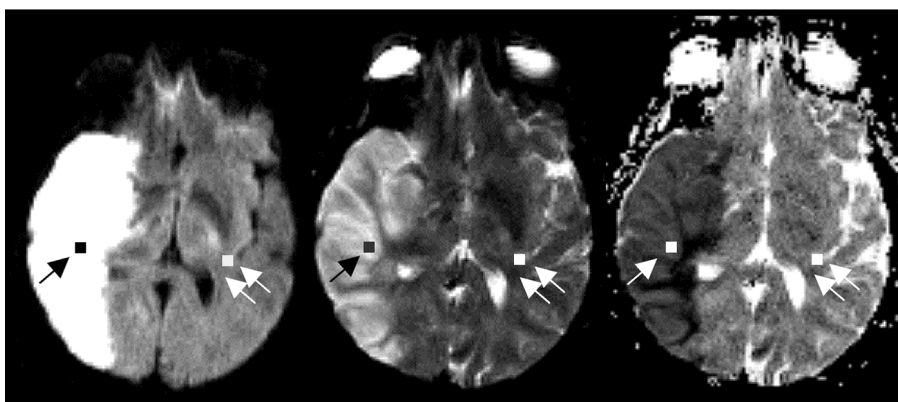


Figure 1. Transverse isotropic diffusion-weighted MR image (left), MR image obtained with low b value (middle), and ADC map (right) in a 51-year-old woman examined 32.6 hours after stroke onset. Note the ROIs (single arrow) placed on the lesion and normal-appearing tissue (double arrows) in the contralateral hemisphere.

ings of neurologic examinations were consistent with a lacunar syndrome.

The lesions on 41 of the 236 images were classified as lacunes. The lesions on 183 images were classified as nonlacunar in etiology. The diagnosis of lacune could be neither established nor excluded for the lesions in the remaining 12 images. Therefore, all 236 images were included in our statistical model that described the data as a whole, but the data from only 224 images (in 139 patients) were included in subgroup analysis in the investigation of the effects of etiology on the time course of ADC.

MR Imaging

MR imaging was performed with a 1.5-T whole-body imaging unit (Signa; GE Medical Systems, Milwaukee, Wis) with a hardware upgrade (Advanced NMR Systems, Wilmington, Mass) for echo-planar imaging that included a catch-and-hold modification. Our diffusion-weighted pulse sequence is based on the pulsed field gradient technique described by Stejskal and Tanner (38) and can be summarized as follows.

T2-weighted single-shot spin-echo images were acquired with repetition time msec/echo time msec of 6,000/118. Diffusion-encoding pulses with duration of 47 msec and interpulse temporal offset of 52 msec were symmetrically placed about the 180° radio-frequency pulse. Additional parameters included a field of view of 40×20 cm and a matrix of 256×128 pixels; 6-mm-thick transverse sections, with 1-mm spacing, were acquired. Diffusion gradients were applied first in a single direction with a low b value of approximately 3 sec/mm^2 (rather than 0

sec/mm^2 , to reduce imaging artifacts), and then they were applied in each of six directions (the minimum necessary to measure the entire diffusion tensor) with a high b value of either 892 or $1,221 \text{ sec/mm}^2$. This series of seven image acquisitions was repeated three times for each section being imaged, so that a total of 21 raw images were acquired for each section. Between 18 and 20 sections were imaged in each patient. The entire diffusion-weighted sequence required 126 seconds of imaging time.

Our postprocessing software averaged the three diffusion tensor data sets to reduce noise and then corrected them for warping effects due to induced eddy currents. They were then used to generate three different images for subsequent analysis. First, isotropic diffusion-weighted images were generated by assigning to each pixel the geometric mean of its signal intensities on the images obtained with a high b value. Second, an image obtained with a low b value was generated by calculating the arithmetic mean of each pixel's signal intensities on the three images obtained with a low b value. This image had almost no diffusion weighting and, therefore, served as a T2-weighted image for purposes of visual analysis. Finally, these two images were used to generate ADC maps. A sample isotropic diffusion-weighted image, an image obtained with a low b value, and an ADC map are shown in Figure 1.

Image Analysis

A neuroradiologist reviewed the diffusion-weighted MR images and images obtained with a low b value on a computer workstation (Sun Microsystems, Mountain View, Calif) with software developed

within the MGH-NMR Center, Boston, and customized for this study by one of the authors (W.A.C.). The number of sections in which an ischemic lesion appeared was recorded to indicate lesion size. The neuroradiologist placed a 3×3 -pixel ROI, corresponding to a 9-voxel region that was 4.69×4.69 mm in plane and 6 mm thick, within each lesion on a single image section. We aimed to place this ROI on the oldest portion of each lesion, that is, the part with an ischemic insult that corresponded to the initial onset of symptoms. Therefore, in accordance with the assumptions that ischemic lesions tend to grow outward from a central core and that cerebral cortex may be most vulnerable to ischemia caused by emboli that lodge proximally, the ROI was placed as close as possible to the anatomic center of the lesion. This was done with the constraint that, when both cortical and deep structures were involved, the ROI was placed near the cortex. To simplify the selection of a contralateral ROI (as discussed later), the ROI was placed as exclusively as possible within either gray matter or white matter, with gray matter selected preferentially when possible.

A second ROI of the same size was placed on normal-appearing brain tissue in the contralateral unaffected side of the brain in the same anatomic location as was the lesion ROI, and this ROI contained roughly the same proportions of gray and white matter. The raw data from a single image section on one image were corrupted by severe artifacts; therefore, the lesion and contralateral ROIs were moved to the closest possible locations on an adjacent image section.

The neuroradiologist reviewing the images was not aware of the time of onset of symptoms in each case. He was, however, informed as to the anatomic location of the lesion, as described in each patient's medical records, to ensure that the lesion chosen was the one that corresponded to the neurologic deficit with a known time of onset rather than to an older or more recent infarct.

For all patients who had more than one image included in this study, the neuroradiologist reviewed these images in chronologic order. This was necessary because, for the second and subsequent images, the lesion ROI was placed in the same anatomic location as it was on the first image. No other information about the patients was available to the reviewing neuroradiologist.

Statistical Analysis

For each image, the mean of the nine ADC values measured in the 3×3 ROI placed on the ischemic lesion was computed. The mean of the nine ADC values measured in the contralateral ROI was also computed. The former result was then divided by the latter to yield the relative ADC (rADC) within the core of the lesion. This single measurement, along with patient information, was transferred to a computer (Macintosh; Apple, Cupertino, Calif) to be analyzed with a commercially available statistical software package (STATA; Stata, College Station, Tex).

Several statistical methods were used. First, to test the hypothesis that rADC continues to decrease rather than remains constant during the first few hours after stroke onset, we fit a simple regression line to a plot of rADC versus time for all images obtained within 12 hours of stroke onset. Second, to provide a preliminary estimate of the stage of stroke evolution at which the lowest rADC occurred, we divided our data into 6-hour periods according to time since onset (eg, 0–6 hours since onset, 6–12 hours since onset) and compared the means of rADC values for lacunes and nonlacunes in each group. Finally, a statistical model was used to predict rADC as a function of time and to test the hypothesis that the evolution of ADC differs according to patient age or stroke etiology. This model included two parts that were used to describe the decrease and subsequent increase in rADC over time. The decrease in rADC was modeled as a linear function of time, beginning with rADC equal to 1 at the time of onset of symptoms. The increase in rADC was modeled as a linear function of the logarithm of time.

This model enabled description of the entire time course of rADC with three parameters: t_t , the time at which transition from decreasing to increasing rADC occurs; $rADC_t$, the value of rADC at that time; and s , the slope of the subsequent increase in rADC. Dummy variables were added to determine age- or etiology-related differences in the time course of ADC that may exist between groups. This model was selected from a variety of competing models because it was the one that best fit the data. The model and the rationale behind its selection are discussed in more detail in the Appendix.

RESULTS

Figure 2 shows the rADC values of all 236

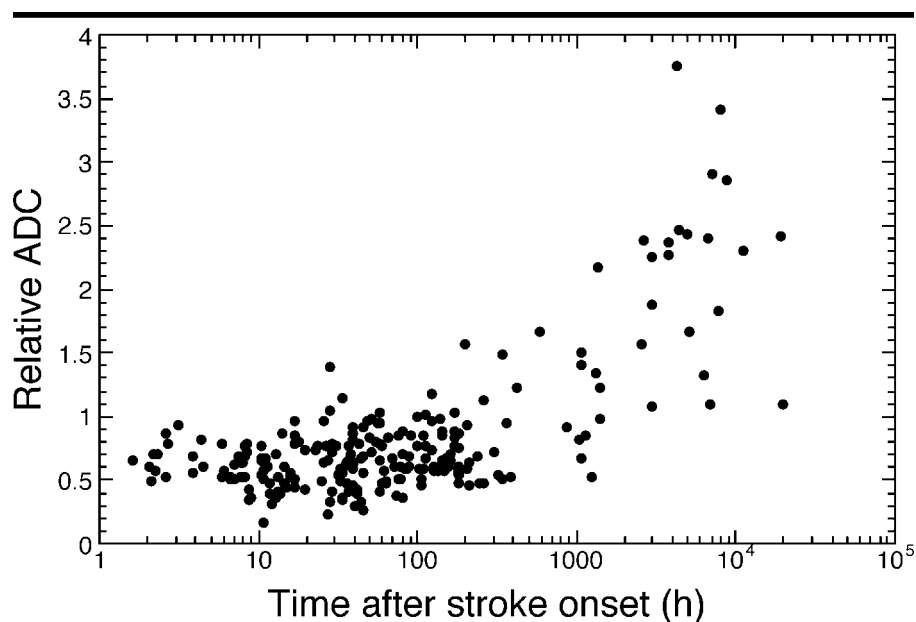


Figure 2. Scatterplot shows time course of rADC in all images. It is apparent that rADC is less than normal (ie, rADC < 1) during the early hours after stroke onset, then increases to pseudo-normal levels, and later increases to elevated levels. rADC does not appear to reach a plateau within the range of time studied.

TABLE 2
rADC in Nonlacunes and Lacunes during the First 2 Days after Stroke Onset

Data	Time after Stroke Onset (h)*							
	0–6	6–12	12–18	18–24	24–30	30–36	36–42	42–48
Nonlacunes								
No. of observations	15	28	12	2	9	7	11	7
Mean rADC	0.680	0.566	0.548	0.755	0.697	0.647	0.678	0.609
SD of rADC	0.135	0.145	0.185	0.023	0.324	0.253	0.157	0.221
Lowest rADC	0.489	0.173	0.354	0.736	0.228	0.352	0.417	0.265
Lacunes								
No. of observations	1	1	5	2	4	5	3	1
Mean rADC	0.605	0.340	0.726	0.579	0.727	0.446	0.452	0.325
SD of rADC†	NA	NA	0.157	0.219	0.324	0.090	0.177	NA
Lowest rADC	0.605	0.340	0.517	0.424	0.407	0.346	0.288	0.325

* For each 6-hour period, the first number is inclusive and the second number is exclusive.

† NA = not applicable.

images included in the study plotted as a function of time. A semilogarithmic plot has been used so that the entire time course can be appreciated with use of one set of axes. This scatterplot shows that rADC is less than normal (ie, <1) on all images obtained within 24 hours of symptom onset. In the earliest observation, at 1.6 hours after stroke onset, the measured rADC was 0.661.

Linear regression of rADC against time for observations ($n = 47$) less than 12 hours after onset yielded a negative slope that was significantly ($P = .009$) different from zero. Further evidence that rADC continues to decrease during the acute period is supported by the fact that sta-

tistical models that incorporated constant rADC during the first phase yielded lower r^2 values than the model that was selected, which describes decreasing rADC.

Table 2 summarizes rADC in each 6-hour period during the first 2 days after stroke onset. Among nonlacunes, the 6-hour period with the lowest mean rADC was the 12–18-hour period (periods with only one observation were excluded from this analysis to avoid excessively weighting a single measurement). Among lacunes, the lowest mean rADC was observed in the 42–48-hour period. Periods with only one lacunar stroke were not excluded, due to the sparseness of data

TABLE 3
Statistical Model of rADC Progression Incorporating Stroke Etiology and Patient Age

Age, Fitted Parameters, and Data	Stroke Etiology	
	Nonlacune	Lacune
≤66.0 y		
Time of transition from decreasing to increasing rADC (h)*	20.2 (2.85)	41.8 (8.94)
Slope of subsequent increase of rADC (log h ⁻¹)†	0.744 (0.058)	0.691 (0.116)
Predicted time of pseudonormalization (h)‡	162	393
No. of images	90	24
>66.0 y		
Time of transition from decreasing to increasing rADC (h)*	13.4 (2.21)	46.2 (12.01)
Slope of subsequent increase of rADC (log h ⁻¹)†	0.507 (0.047)	0.825 (0.119)
Predicted time of pseudonormalization (h)‡	282	301
No. of images	93	17

Note.—The computed value of rADC_t was 0.328 (standard error, 0.0397), and it was significantly different from 1 ($P < .001$). No evidence for between-group differences in rADC_t was found.

* Data in parentheses are standard errors. The time of transition was significantly later ($P = .02$) for lacunes than for nonlacunes. There was a trend toward earlier transition in patients older than the median age of 66.0 years compared with younger patients ($P = .06$). There was no significant interaction of age and etiology with respect to time of transition ($P = .47$).

† Data in parentheses are standard errors. The slope was measured in an rADC increase per a factor of 10 increase in time (see Fig 3). There was a significant interaction ($P = .03$) of age and etiology with respect to slope. Among nonlacunes, slope was significantly greater ($P = .001$) in younger than in older patients. There was no significant effect of age on slope among lacunes ($P = .37$).

‡ The predicted time of pseudonormalization was computed indirectly from the fitted parameters for each group of images.

from lacunes, which is clearly evident in Table 2.

When the statistical model was fit to all 236 images as a single group, the estimated transition from decreasing to increasing rADC occurred at 18.5 hours after stroke onset (the standard error of this parameter was 1.82 hours). The estimated rADC at the time of transition from decreasing to increasing rADC was 0.339 (standard error, 0.039), a value that was significantly different from 1 ($P < .001$). The subsequent slope of the increase of rADC was 0.619 per factor of 10 increase in time (standard error, 0.038). This implies that pseudonormalization occurs at 216 hours, or 9 days after stroke onset.

The results of fitting an expanded model, including dummy variables representing stroke etiology and patient age, are shown in Table 3. No significant between-group differences were detected in the value of rADC at the time of transition. Therefore, the three terms representing such differences were eliminated from the model (Appendix). The computed transition from decreasing to increasing rADC occurred later in lacunes than in nonlacunes ($P = .02$). There was a trend toward earlier transition in older compared with younger patients ($P = .06$). There was no significant interaction between age and etiology with respect to the time of transition.

With respect to the slope of subsequent increase of rADC, there was a significant interaction ($P = .03$) of age and etiology. To clarify the implications of this interaction, separate reanalyses of each etiologic subgroup were performed. Among nonlacunes, the slope was significantly greater ($P = .001$) for younger patients than it was for older patients. However, among lacunes, the estimated slope was slightly greater for older patients than it was for younger patients, though the difference was not statistically significant ($P = .37$). The lack of a significant effect could be due to the small number of lacunes sampled.

The time at which pseudonormalization was computed to take place in each group of patients is also included in Table 3. Statistical inference regarding differences between pseudonormalization times is complicated by the fact that these values are derived from the three fitted parameters and, therefore, are determined by using the model only indirectly.

All lacunes are small lesions, but nonlacunes can be of any size. Therefore, lacunar etiology is confounded with lesion size. To rule out the possibility that the previously described difference in transition time between lacunes and nonlacunes was due to lesion size, rather than to lesion etiology per se, the model was fit again, including only those 107 images in which the observed lesion

spanned fewer than five image sections (these images depicted 41 lacunes and 66 nonlacunes). Again, the transition from decreasing to increasing rADC occurred later for lacunes ($P = .04$). The remainder of this limited model with 107 observations is not reproduced here.

DISCUSSION

The data in this study confirm the data of numerous previous studies in which the stereotypical time course of ADC changes in stroke has been established and extend the findings of these studies by sampling a larger group of patients. As in previous human studies, our study is limited by the fact that the time when a patient first exhibited a new neurologic deficit usually cannot be determined exactly from medical records. We address this limitation explicitly by specifying a degree of precision with which we required that stroke onset times be known.

Data in this study also extend findings of earlier studies by documenting that minimum ADC may be reached more rapidly in the core of nonlacunes than in the core of lacunes and by suggesting that minimum ADC may be reached more rapidly in older patients. Researchers (28,31) in animal studies have found that attainment of minimum ADC may coincide with the emergence of eosinophilic neurons and the beginning of neuronal necrosis. It has been suggested that the rebound of ADC beginning at this time represents the loss of cell membrane integrity, with consequent removal of restrictions on water diffusion. In light of this idea, the current findings may signify that an important pathologic milestone is reached more slowly in lacunar infarcts and in younger patients. If so, there may be a relatively longer therapeutic window of opportunity in younger patients and in those whose strokes are lacunes. It is possible that earlier transition to increasing rADC in nonlacunes may occur in part because many of them are embolic, and reperfusion may occur more frequently in embolic stroke.

This study also extends the findings of previous work by suggesting that the rate of subsequent increase in ADC in nonlacunes is more rapid in younger patients, although we did not detect such a difference in lacunar infarcts. The rebound of ADC is likely due in large part to loss of cell membrane integrity, vasogenic edema, and finally gradual phagocytosis of necrotic debris. It has been shown (39) that therapeutic reperfusion may hasten

pseudonormalization. This suggests that the observed age-related differences in time of transition from decreasing to increasing ADC and in the rate of rebound of ADC could be explained by more frequent occurrence of spontaneous reperfusion in younger patients, perhaps through more effective collateral circulation. Accordingly, the lack of an effect of age on the time of transition in lacunes could be explained by the fact that lacunar infarctions occur in end-arterial territory without collateral circulation. Future research could be directed toward an investigation of these hypotheses by correlating the rate of change in ADC with angiographic evidence of collateral circulation. If proven, an effect of collateral circulation on ADC progression could support the use of angiography, or perhaps perfusion-weighted MR imaging or computed tomography, prior to administration of thrombolytic agents. Alternatively, the effect of age on the rebound of ADC could be explained by a more brisk inflammatory response in younger patients.

The conclusions of this study are limited by the problem that smaller lesions may cause neurologic deficits that are less severe or that fluctuate in severity and, therefore, may have a less precisely defined time of onset. Furthermore, our conclusions regarding differences between lacunar and nonlacunar infarcts are limited by the fact that lesion etiology is partially confounded by lesion size. We sought to control for this confounding factor by repeating our analysis of etiology-related differences with a subset of the data containing only smaller lesions. Future research that incorporates explicit study of the effect of lesion size on the time course of ADC could address this issue more directly.

Further refinement of our model could provide more accurate prediction of rADC during the first few hours after stroke onset. Although we used a linear model for the decrease in rADC in the first few hours after stroke onset, our data suggest that this decrease is actually nonlinear, with a brief period of rapid decrease, which was complete before the first of our observations was obtained at 1.6 hours after stroke onset, followed by several hours of less rapid decrease. Such a process, in theory, could be described by an exponential or biexponential model; however, competing models including exponential or biexponential decrease fit our data much less well than the selected model.

Because of this limitation of our initial

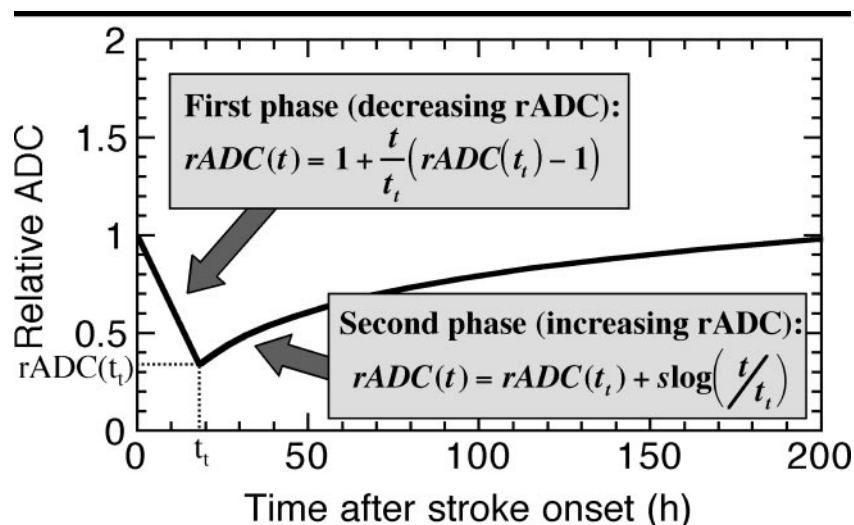


Figure 3. Statistical model shows equations used to predict rADC. The model incorporates a first phase of linearly decreasing rADC and a second phase of logarithmically increasing rADC. The model can be used to predict rADC as a function of time after stroke onset, or t , with the following three fitted parameters: t_t , the time of transition between decreasing and increasing rADC; $rADC_{t_t}$, the computed rADC at that time; and s , the slope of subsequent rADC increase.

model, its valid uses include predicting the time at which minimum rADC is reached in a group of patients, on the basis of fitting a group of observations, but not predicting the rADC value in an individual acute stroke at a given time after stroke onset.

Finally, another potential extension of this research would be measurement of ADC within different parts of a developing ischemic lesion. With our method, like those of previous studies in which ADC was measured within a large ROI or within the entire lesion, heterogeneity of ADC within a developing lesion could not be identified. Because ischemic lesions usually grow to a size larger than that observed in acute-stage diffusion-weighted MR imaging (14,40–44), it is reasonable to assume that such heterogeneity evolves as initially normal tissue is recruited into a growing infarct, with the newly recruited tissue exhibiting a decrease in ADC that begins some time after the decrease in ADC in the original core of the lesion. Indeed, substantial heterogeneity of ADC values has been shown (13) to exist even at a single time within acute infarcts. The time course of ADC in the expanding rim of a lesion has not been described, to our knowledge.

In summary, our data confirm, in a larger and more precisely characterized group of patients, findings of earlier studies that show a stereotypical time course for ADC changes and further demonstrate heterogeneity of this time course

among patient populations. Our initial data suggest that the initial evolution of lacunes is slower than that of nonlacunes. They also suggest that ischemic tissue damage may occur more rapidly in older patients. Finally, they suggest that older patients have a slower rate of pseudonormalization than do younger patients. Further investigation into the heterogeneity of the ADC time course, correlated with clinical outcomes and possibly with therapeutic interventions, may allow ADC to become a useful tool in rational stroke therapy.

APPENDIX

To provide the best description of the data, eight competing statistical models were fit to the entire set of 236 observations. Each of these models featured two parts; the first described the decrease in rADC from its initial value of 1 to a minimum value, and the second described the subsequent increase in rADC. The eight competing models represented all combinations of four possible equations for the first phase (linear, exponential, biexponential, and constant) and two possible equations for the second phase (linear and logarithmic). In every model except that with a constant first phase, the first phase was constrained such that predicted rADC was 1 at the time of stroke onset. In all models tested, between three and six parameters were used.

The r^2 values obtained by fitting each model were compared, and the best fit was

obtained with the three-parameter model that specified linear decrease followed by logarithmic increase ($r^2 = 0.87$, $P < 10^{-6}$). Therefore, this model was used for statistical analysis. It is summarized in greater detail in Figure 3. Fitting the other seven competing models yielded r^2 values no greater than 0.64.

After a model was selected, three dummy variables, which represented age, etiology, and the interaction between them, were added to this model to detect differences in the time course of ADC that may exist between groups. For example, t_t , the variable that represents the time of transition from decreasing to increasing rADC (Fig 3), was replaced by the expression $t_{t[younger, nonlacune]} + (x_{lacune} \Delta t_{t, lacune}) + (x_{older} \Delta t_{t, older}) + (x_{both} \Delta t_{t, both})$, where x_{lacune} and x_{older} are set to 1 for lacunes and older patients, respectively, and zero otherwise; x_{both} is set to 1 only for lacunes that occur in older patients, to reflect the interaction between age and etiology; and the Δt_t terms represent group-related differences in t_t . All three Δt_t parameters, as well as the three $\Delta rADC_t$ parameters and the three Δs parameters, were fit by using the model so that incorporation of three dummy variables increased the number of parameters to be fit from three to 12.

Constructing the model in this way allowed determination of significant between-group differences in any of the three basic parameters of the model. For example, in the previously mentioned expression, if the fitted value of $\Delta t_{t, lacune}$ is positive and significantly different from zero, this implies that t_t is reached later for lacunes compared with nonlacunes.

Because none of the $\Delta rADC_t$ parameters was significantly different from zero, these were eliminated from the model, which resulted in a final model with nine fitted parameters. The parameters in Table 3 are those obtained by fitting this model.

Acknowledgment: The authors thank Elkan Halpern, PhD, Department of Radiology, Massachusetts General Hospital Decision Analysis and Technology Assessment Group, Boston, for his assistance with statistical analysis.

References

1. Lövblad KO, Laubach HJ, Baird AE, et al. Clinical experience with diffusion-weighted MR in patients with acute stroke. *AJNR Am J Neuroradiol* 1998; 19:1061–1066.
2. Singer MB, Chong J, Lu D, Schonewille WJ, Tuhim S, Atlas SW. Diffusion-weighted MRI in acute subcortical infarction. *Stroke* 1998; 29:133–136.
3. Gonzalez RG, Schaefer PW, Buonanno FS, et al. Diffusion-weighted MR imaging: diagnostic accuracy in patients imaged within 6 hours of stroke symptom onset. *Radiology* 1999; 210:155–162.
4. Moseley ME, Kucharczyk J, Mintorovitch J, et al. Diffusion-weighted MR imaging

- of acute stroke: correlation with T2-weighted and magnetic susceptibility-enhanced MR imaging in cats. *AJNR Am J Neuroradiol* 1990; 11:423–429.
5. Moseley ME, Cohen Y, Mintorovitch J, et al. Early detection of regional cerebral ischemia in cats: comparison of diffusion- and T2-weighted MRI and spectroscopy. *Magn Reson Med* 1990; 14:330–346.
6. Davis D, Ulatowski J, Eleff S, et al. Rapid monitoring of changes in water diffusion coefficients during reversible ischemia in cat and rat brain. *Magn Reson Med* 1994; 31:454–460.
7. Pierpaoli C, Alger JR, Righini A, et al. High temporal resolution diffusion MRI of global cerebral ischemia and reperfusion. *J Cereb Blood Flow Metab* 1996; 16:892–905.
8. Yoneda Y, Tokui K, Hanihara T, Kitagaki H, Tabuchi M, Mori E. Diffusion-weighted magnetic resonance imaging: detection of ischemic injury 39 minutes after onset in a stroke patient. *Ann Neurol* 1999; 45:794–797.
9. Warach S, Chien D, Li W, Ronthal M, Edelman RR. Fast magnetic resonance diffusion-weighted imaging of acute human stroke. *Neurology* 1992; 42:1717–1723.
10. Warach S, Gaa J, Siewert B, Wielopolski P, Edelman RR. Acute human stroke studied by whole brain echo planar diffusion-weighted magnetic resonance imaging. *Ann Neurol* 1995; 37:231–241.
11. Lutsep HL, Albers GW, DeCrespigny A, Kamat GN, Marks MP, Moseley ME. Clinical utility of diffusion-weighted magnetic resonance imaging in the assessment of ischemic stroke. *Ann Neurol* 1997; 41:574–580.
12. Schlaug G, Siewert B, Benfield A, Edelman RR, Warach S. Time course of the apparent diffusion coefficient (ADC) abnormality in human stroke. *Neurology* 1997; 49:113–119.
13. Nagesh V, Welch KM, Windham JP, et al. Time course of ADCw changes in ischemic stroke: beyond the human eye. *Stroke* 1998; 29:1778–1782.
14. Schwamm LH, Koroshetz WJ, Sorensen AG, et al. Time course of lesion development in patients with acute stroke: serial diffusion- and hemodynamic-weighted magnetic resonance imaging. *Stroke* 1998; 29:2268–2276.
15. Yang Q, Tress BM, Barber PA, et al. Serial study of apparent diffusion coefficient and anisotropy in patients with acute stroke. *Stroke* 1999; 30:2382–2390.
16. Beaulieu C, de Crespigny A, Tong DC, Moseley ME, Albers GW, Marks MP. Longitudinal magnetic resonance imaging study of perfusion and diffusion in stroke: evolution of lesion volume and correlation with clinical outcome. *Ann Neurol* 1999; 46:568–578.
17. Hossmann KA. Cortical steady potential, impedance and excitability changes during and after total ischemia of cat brain. *Exp Neurol* 1971; 32:163–175.
18. Benveniste H, Hedlund LW, Johnson GA. Mechanism of detection of acute cerebral ischemia in rats by diffusion-weighted magnetic resonance microscopy. *Stroke* 1992; 23:746–754.
19. Siesjö BK. Pathophysiology and treatment of focal cerebral ischemia. I. Pathophysiology. *J Neurosurg* 1992; 77:169–184.
20. Szafer A, Zhong J, Gore JC. Theoretical model for water diffusion in tissues. *Magn Reson Med* 1995; 33:697–712.
21. Anderson AW, Zhong J, Petroff OA, et al. Effects of osmotically driven cell volume changes on diffusion-weighted imaging of the rat optic nerve. *Magn Reson Med* 1996; 35:162–167.
22. van der Toorn A, Sykova E, Dijkhuizen RM, et al. Dynamic changes in water ADC, energy metabolism, extracellular space volume, and tortuosity in neonatal rat brain during global ischemia. *Magn Reson Med* 1996; 36:52–60.
23. Dijkhuizen RM, de Graaf RA, Tulleken KA, Nicolay K. Changes in the diffusion of water and intracellular metabolites after excitotoxic injury and global ischemia in neonatal rat brain. *J Cereb Blood Flow Metab* 1999; 19:341–349.
24. Neil JJ, Duong TQ, Ackerman JJ. Evaluation of intracellular diffusion in normal and globally-ischemic rat brain via 133Cs NMR. *Magn Reson Med* 1996; 35:329–335.
25. Duong TQ, Ackerman JJ, Ying HS, Neil JJ. Evaluation of extra- and intracellular apparent diffusion in normal and globally ischemic rat brain via 19F NMR. *Magn Reson Med* 1998; 40:1–13.
26. Helpert JA, Ordidge RJ, Knight RA. The effect of cell membrane water permeability on the apparent diffusion coefficient of water (abstr). In: Book of abstracts: Society of Magnetic Resonance in Medicine 1992. Berkeley, Calif: Society of Magnetic Resonance in Medicine, 1992; 1201.
27. Takahashi M, Fritz-Zieroth B, Chikugo T, Ogawa H. Differentiation of chronic lesions after stroke in stroke-prone spontaneously hypertensive rats using diffusion weighted MRI. *Magn Reson Med* 1993; 30:485–488.
28. Welch KM, Windham J, Knight RA, et al. A model to predict the histopathology of human stroke using diffusion and T2-weighted magnetic resonance imaging. *Stroke* 1995; 26:1983–1989.
29. Matsumoto K, Lo EH, Pierce AR, Wei H, Garrido L, Kowall NW. Role of vasogenic edema and tissue cavitation in ischemic evolution on diffusion-weighted imaging: comparison with multiparameter MR and immunohistochemistry. *AJNR Am J Neuroradiol* 1995; 16:1107–1115.
30. Jiang Q, Zhang ZG, Chopp M, et al. Temporal evolution and spatial distribution of the diffusion constant of water in rat brain after transient middle cerebral artery occlusion. *J Neurol Sci* 1993; 120:123–130.
31. Helpert JA, Dereski MO, Knight RA, Ordidge RJ, Chopp M, Qing ZX. Histopathological correlations of nuclear magnetic resonance imaging parameters in experimental cerebral ischemia. *Magn Reson Imaging* 1993; 11:241–246.
32. Knight RA, Dereski MO, Helpert JA, Ordidge RJ, Chopp M. Magnetic resonance imaging assessment of evolving focal cerebral ischemia: comparison with histopathology in rats. *Stroke* 1994; 25:1252–1261.
33. Clavier I, Hommel M, Besson G, Noelle B, Perret JE. Long-term prognosis of symptomatic lacunar infarcts: a hospital-based study. *Stroke* 1994; 25:2005–2009.
34. Adams HP Jr, Davis PH, Leira EC, et al.

- Baseline NIH Stroke Scale score strongly predicts outcome after stroke: a report of the Trial of Org 10172 in Acute Stroke Treatment (TOAST). *Neurology* 1999; 53:126–131.
35. Nakayama H, Jorgensen HS, Raaschou HO, Olsen TS. The influence of age on stroke outcome: the Copenhagen stroke study. *Stroke* 1994; 25:808–813.
 36. Jorgensen HS, Reith J, Nakayama H, Kammergaard LP, Raaschou HO, Olsen TS. What determines good recovery in patients with the most severe strokes? the Copenhagen stroke study. *Stroke* 1999; 30:2008–2012.
 37. Adams HP Jr, Bendixen BH, Kappelle LJ, et al. Classification of subtype of acute ischemic stroke: definitions for use in a multicenter clinical trial—TOAST: Trial of Org 10172 in Acute Stroke Treatment. *Stroke* 1993; 24:35–41.
 38. Stejskal E, Tanner J. Spin diffusion measurements: spin echoes in the presence of a time-dependent field gradient. *J Chem Phys* 1965; 42:288–292.
 39. Kidwell CS, Saver JL, Mattiello J, et al. Thrombolytic reversal of acute human cerebral ischemic injury shown by diffusion/perfusion magnetic resonance imaging. *Ann Neurol* 2000; 47:462–469.
 40. Sorensen AG, Buonanno FS, Gonzalez RG, et al. Hyperacute stroke: evaluation with combined multisection diffusion-weighted and hemodynamically weighted echo-planar MR imaging. *Radiology* 1996; 199:391–401.
 41. Baird AE, Benfield A, Schlaug G, et al. Enlargement of human cerebral ischemic lesion volumes measured by diffusion-weighted magnetic resonance imaging. *Ann Neurol* 1997; 41:581–589.
 42. Barber PA, Darby DG, Desmond PM, et al. Prediction of stroke outcome with echo-planar perfusion- and diffusion-weighted MRI. *Neurology* 1998; 51:418–426.
 43. van Everdingen KJ, van der Grond J, Kappelle LJ, Ramos LM, Mali WP. Diffusion-weighted magnetic resonance imaging in acute stroke. *Stroke* 1998; 29:1783–1790.
 44. Sorensen AG, Copen WA, Østergaard L, et al. Hyperacute stroke: simultaneous measurement of relative cerebral blood volume, relative cerebral blood flow, and mean tissue transit time. *Radiology* 1999; 210:519–527.